Cochlear Outer Hair Cell Bending in an External Electric Field

Gregory I. Frolenkov,# Federico Kalinec,* George A. Tavartkiladze,# and Bechara Kachar*
*Section on Structural Cell Biology, National Institute on Deafness and Other Communication Disorders, National Institutes of Health, Bethesda, Maryland 20892 USA, and #Department of Experimental and Clinical Audiology, Research Center for Audiology and Hearing Rehabilitation, Moscow, Russia

ABSTRACT We have used a high-resolution motion analysis system to reinvestigate shape changes in isolated guinea pig cochlear outer hair cells (OHCs) evoked by low-frequency (2–3 Hz) external electric stimulation. This phenomenon of electromotility is presumed to result from voltage-dependent structural changes in the lateral plasma membrane of the OHC. In addition to well-known longitudinal movements, OHCs were found to display bending movements when the alternating external electric field gradients were oriented perpendicular to the cylindrical cell body. The peak-to-peak amplitude of the bending movement was found to be as large as 0.7 μm. The specific sulfhydryl reagents, *p*-chloromercuriphenylsulfonic acid and *p*-hydroxymercuriphenylsulfonic acid, that suppress electrically evoked longitudinal OHCs movements, also inhibit the bending movements, indicating that these two movements share the same underlying mechanism. The OHC bending is likely to result from an electrical charge separation that produces depolarization of the lateral plasma membrane on one side of the cell and hyperpolarization on the other side. In the cochlea, OHC bending could produce radial distortions in the sensory epithelium and influence the micromechanics of the organ of Corti.

INTRODUCTION

An ATP-independent (Kachar et al., 1986), membrane-based motility (Kalinec et al., 1992), which follows cycle by cycle the transitions in an electric field (Kachar et al., 1986; Ashmore, 1987), is responsible for at least part of the in vitro experimental observations of outer hair cell (OHC) motility (Brownell et al., 1985; Zenner et al., 1985). This novel putative mechanism of membrane-based motility is driven by changes in plasma membrane potential (Santos-Sacchi and Dilger, 1988; Iwasa and Kachar, 1989; Dallos et al., 1991) and results from conformational changes of putative motor elements in the lateral plasma membrane (Kalinec et al., 1992).

OHC motility is widely believed to play a crucial role in mechano-electro-mechanical feedback, called "cochlear amplification," which is responsible for the fine-tuning and sensitivity of the mammalian cochlea (see Brownell and Kachar, 1985; Patuzzi and Robertson, 1988). Sound coming into the cochlea is known to produce displacement of the basilar membrane, initiating a "traveling wave" along this membrane (von Békésy, 1960). Because of the geometry of the organ of Corti, any motion of the basilar membrane in the transverse direction evokes a shear displacement between the apical surfaces of OHCs and the overlying tectorial membrane, producing deflection of OHC stereocilia bundles that are mechanically coupled to the tectorial membrane. This deflection modifies the electrical conductance of mechanosensitive channels associated with the stereocilia and results in the modulation of current passing into the OHC. This effect changes OHC intracellular potential, causing the OHC to generate force. It was recently demonstrated in vitro that stereocilia deflections can induce OHC motility (Evans and Dallos, 1993).

However, it is difficult to understand how the proposed cochlear amplifier mechanism could work at high frequencies because of the attenuation of cycle-by-cycle receptor potential changes (Santos-Sacchi, 1992; Kolston, 1995). Indeed, as observed in OHCs from basal turns (high-frequency region) of the intact organ of Corti, the sound-induced receptor potential changes start to decline at frequencies significantly less than the characteristic frequencies (Dallos and Cheatham, 1992). This decline is associated with the charging of the OHC membrane capacitance, which results in a reduction of OHC motility (Santos-Sacchi, 1992). Several ideas have been proposed that could explain this phenomenon. Dallos and Evans, for example, have suggested that extracellular potential variations resulting from transduction current changes could be a driving force for high-frequency OHC motility in vivo (Dallos and Evans, 1995). Whether or not this is true, an extracellular electric field can clearly modify the OHC motile response.

Recent studies of OHC electrokinetic shape changes in an external electric field (Evans et al., 1991; Hallworth et al., 1993; Dallos and Evans, 1995) have considered changes only in the longitudinal direction. The spatial orientation of the electric fields that around OHCs and associated with the transduction currents is not known. In the organ of Corti, the cylindrical cell bodies of OHCs are oriented at an angle in relation to the reticular lamina (Spoendlin, 1970) and could be exposed to both the longitudinal and perpendicular components of an electric field. We now report that in addition to elongation and shortening, isolated OHCs can also ex-

Received for publication 7 March 1997 and in final form 21 May 1997.
Address reprint requests to Dr. Bechara Kachar, Section on Structural Cell Biology, NIDCD, Rm. 5D15, Bldg. 36, National Institutes of Health, Bethesda, MD 20892. Tel.: 301-402-1600; Fax: 301-402-1765; E-mail: kachar@pop.nidcd.nih.gov.

0006-3495/97/09/1665/08 $2.00

hibit bending movements when exposed to an external electric field perpendicular to their cell bodies. In the organ of Corti, such bending movements could produce radial shear stresses that modulate the OHC-based amplification mechanism.

MATERIALS AND METHODS

OHC isolation

Adult guinea pigs (200–400 g) were sedated with carbon dioxide and decapitated. The temporal bones were removed from the skull and placed in Leibowitz L-15 cell culture medium (National Institutes of Health media unit, pH 7.2, osmolarity 320 ± 5 mmol/kg). The bulla was opened to expose the cochlea, and the otic capsule was then chipped away with a surgical blade, starting from the base. Strips of the organ of Corti were dissected from the cochlea with a fine needle and transferred with a glass pipette into 100 μl of L-15 containing 1 mg/ml collagenase (type IV; Life Technologies, New York). After 10–15 min of incubation, the tissue was transferred into 100 μl of collagenase-free L-15 on a glass microscope slide, and the cells were dissociated by reflux of the tissue through the needle of a Hamilton syringe (no. 705, 22 gauge; Hamilton, Reno, NV). Motility studies were initiated after allowing isolated OHCs to settle for 5 min. Cells used in this study ranged from 55 μm to 90 μm in length. Cells were maintained throughout the experiment in 100 μl medium in an open chamber on the surface of a thin microscope slide at room temperature (20–23°C). Osmolarity measurements showed that the addition of small droplets of distilled water (15 μl) to the chamber every 15 min compensates for the evaporation of water in our experimental conditions. This procedure was routinely used in the experiments.

Electric field stimulation

Two Ag-AgCl pellets (1 mm diameter) were inserted by manipulators into the open chamber containing OHCs and placed 2 ± 0.2 mm apart, across the diameter of the frontal lens of the objective (Fig. 1). Alternating voltage changes were applied between the pellets through a generator with an output resistance of 50 Ω. Voltage changes were kept at 1–2 V, producing a voltage gradient of 0.5–1 mV/μm and a net current in the fluid of 2.6–5.2 mA. At these current levels, only movements of the OHCs were observed. Electrophoretic movements of the smallest observable extracellular debris were only seen with currents of at least 8 mA, well above the experimental conditions. Because the distance between the electrodes (2 mm) was at least two orders of magnitude larger than the diameter of the OHC (10 μm), we presume that the electric field across the cell is uniform (Fig. 1). In fact, we did not detect differences in our observations when we moved the cell up to 200 μm away from the middle point between the electrodes.

Electrodes were placed in fixed positions to the left and right of the microscopic field of view. Alignment of the OHC axis at different angles in relation to the direction of the electric field was produced by rotating the microscope stage. Each OHC was tested with a longitudinal electric field (0°) and two perpendicular positions (+90° and −90°). For each cell, square pulses were used to measure movement amplitude, and sinusoidal bursts were used to test movement nonlinearity.

Light microscopy and OHC motility measurements

A Zeiss Axiomat inverted microscope with an internally corrected 50×, 1.0 numerical aperture (n.a.) objective or a 100×, 1.3 n.a. planapochromatic objective was used in the differential interference contrast (DIC) mode. A 0.63-n.a. condenser was fully illuminated with a 100-W Hg lamp aligned for critical illumination (Kachar et al., 1987). Video clips (3 s or 10 s) of OHC movements were recorded with a video camera (DAGE-MTI, Michigan City, IN) and an optical disk recorder (Panasonic TQ-3031F) for subsequent off-line movement quantification with the image processing and analysis system IMAGE 1 (Universal Imaging, West Chester, PA).

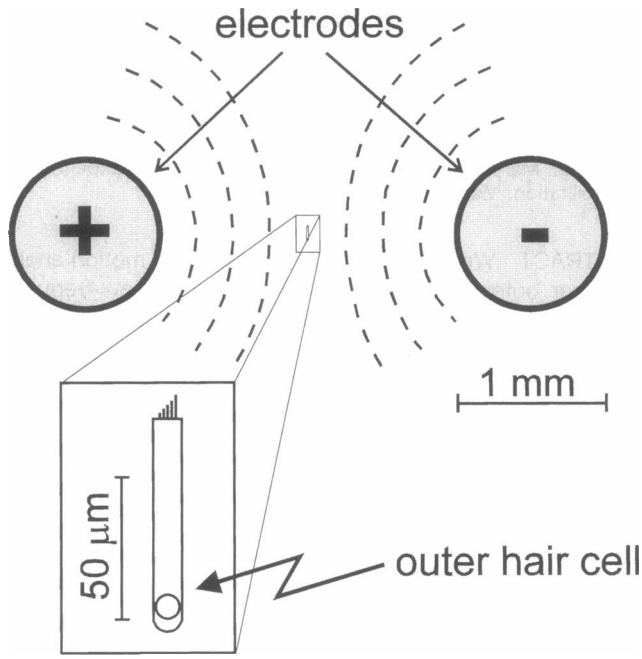

FIGURE 1 Schematic illustration showing the position and size of the electrodes. The dashed lines are an approximation of the lines of constant potentials.

The movements of 27 OHCs were analyzed. The direction of the shear (shading) in the DIC image was adjusted to enhance the contrast and definition of the moving portions of the cell. Quantification of the movement was done on the digitized images by placing a measuring rectangle arbitrarily positioned perpendicularly across the moving edge of the cell (Fig. 2). The rectangle ranged in length from 5 μm to 10 μm and was composed of 3–15 rows of pixels for each frame. Wider measuring rectangles (15–50 rows of pixels) were used for the edges with less contrast. The intensity of the pixel brightness (in arbitrary units) along these lines was averaged and plotted. The number of points in each intensity profile was increased 10 times with the mathematical procedure of cubic spline interpolation (Korn and Korn, 1968). Movements of the cell edge were calculated from shifts in the steep brightness intensity profiles (Fig. 2). Values for this shift were obtained by the least-squares procedure (Korn and Korn, 1968). We tested our motion detection method on small particles in Brownian motion, and we were able to monitor movements of amplitude as small as 0.02 μm.

Sulfhydryl agent application

Stock solutions (50 mM) of *p*-chloromercuriphenylsulfonic acid (pCMPS) and *p*-hydroxymercuriphenylsulfonic acid (pHMPS) (Sigma Chemical Co., St. Louis, MO) in distilled water were used. Solution osmolarities were adjusted to 320 mmol/kg with D-glucose. After OHC movement in perpendicular and longitudinal electric fields was recorded, 2 μl of pCMPS or pHMPS stock solution was added to L-15 medium for a final concentration of 1 mM. Stock solution (2–10 μl) was added to the experimental chamber at a distance 2–10 mm from the cell under investigation.

RESULTS

The characteristic elongation and shortening of isolated OHCs exposed to alternating transcellular voltage gradients

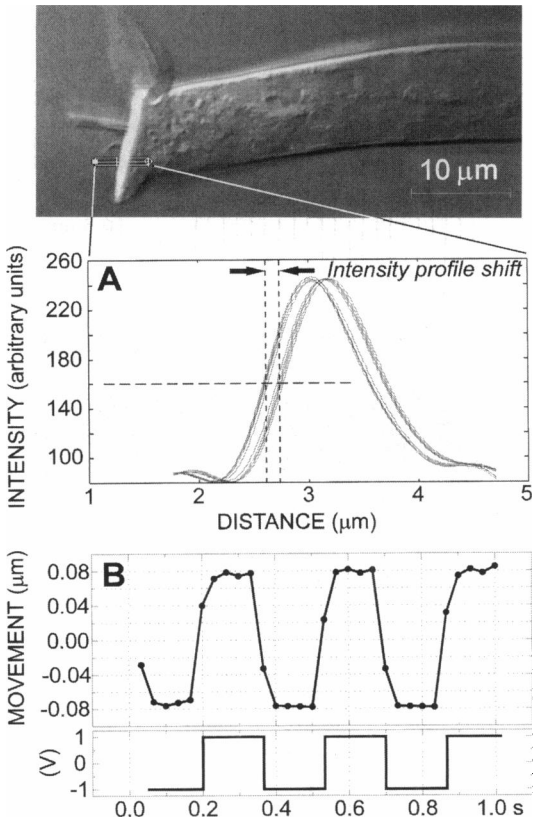

FIGURE 2 Quantification of outer hair cell (OHC) movement. The top panel shows the apical half of an OHC. The small area of image enclosed by white lines represents the measuring rectangle arbitrarily aligned across the cuticular plate. The mean brightness was calculated for each vertical column of pixels inside the measuring rectangle. Changes in brightness along the measuring rectangle are shown in *A*. The curves correspond to superimposed intensity profiles calculated from 10 consecutive frames. (*B*) Movement of the cuticular plate along the *x* axis obtained as a frame-by-frame shift of intensity profiles. The square pulse stimulation is shown at the bottom. Pulses had a frequency of 3 Hz and an amplitude of 1 V, corresponding to a potential gradient of ~0.5 mV/μm.

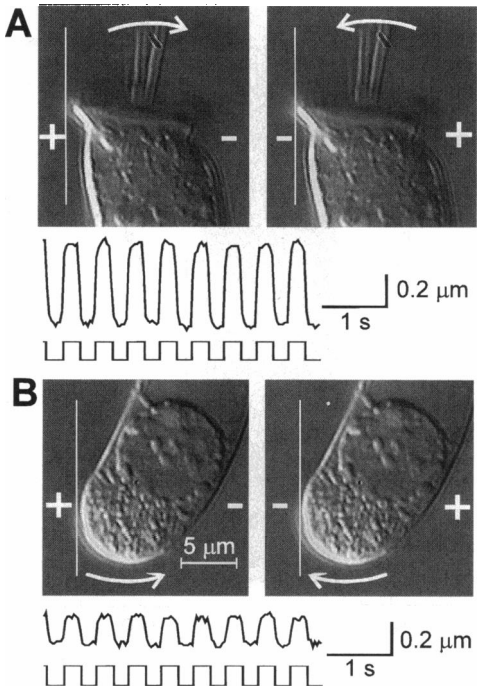

FIGURE 3 Electrically evoked bending of apical (*A*) and basal (*B*) poles of the OHC. The images on the left of *A* and *B* were taken when current was passing from the left electrode to the right one (the electric field direction is marked by *plus and minus signs*). The images on the right side of *A* and *B* were taken when the electric field was passing from the right electrode to the left one. Arrows indicate the direction of movement relative to the vertical reference line. The measurement rectangle was aligned to quantify the movement along the *x* axis of the stereocilia (*A*) and the nuclear pole (*B*). At the bottom of *A* and *B* we show the movements and the stimulating square pulses (2 Hz, 2 V; the corresponding potential gradient is ~1 mV/μm).

could be measured to a very fine degree of resolution with our motion detection method (Fig. 2). When the same voltage gradients were applied in a direction perpendicular to the axis of the OHC, it produced lateral distortions of the cylindrical cell body (Fig. 3). Like the well-characterized axial OHC shape changes, the form and amplitude of lateral distortions depended on how the individual cells where attached to the substrate. If the middle of the OHC body was attached to the microscopic glass slide (as indicated in Fig. 4 by the bracketed area), then both the apical and basal poles of the cell would bend simultaneously in the same direction, following cycle by cycle the electric stimulus (Fig. 3, *A* and *B*). Bending of OHCs occurred to both the left and right, irrespective of the particular cell curvature or cuticular plate tilting angle. The apical and basal poles of the cell were always displaced toward the negative electrode. When the cell was rotated 90°, so the cell body would be parallel to the electric field, the bending motion was replaced by characteristic shortening and elongation (Fig. 5). The displacements of the ends of the cell were in antiphase (Fig. 5). The cell contracted (Fig. 5) when the electric field was directed from the cuticular plate to the basal region and elongated (Fig. 5) when the electric field was applied in the opposite direction.

To analyze the movement as a function of the distance from the point of bending, we measured displacements at different points for the cell shown in Fig. 3. The results plotted in Fig. 4 show an angle of bending of 0.0053 radians for the apical portion of the cell and 0.0024 radians for the basal portion.

Under maximum stimulating voltage (2 V), the amplitude of the bending at the cell distal ends never exceeded 0.7 μm (peak to peak), even for the longest (~90 μm) cells. The bending was visible in all OHCs with well-preserved cylindrical shape. However, electrically evoked bending was less visible in cells with decreased turgor and was not observed in damaged cells.

The amplitude of the longitudinal response varied more between cells than did the bending response. Under maximum interelectrode potential difference (2 V, 1 mV/μm voltage gradient), the amplitude of the longitudinal movements varied from 0.1 to 1.1 μm between the 27 cells

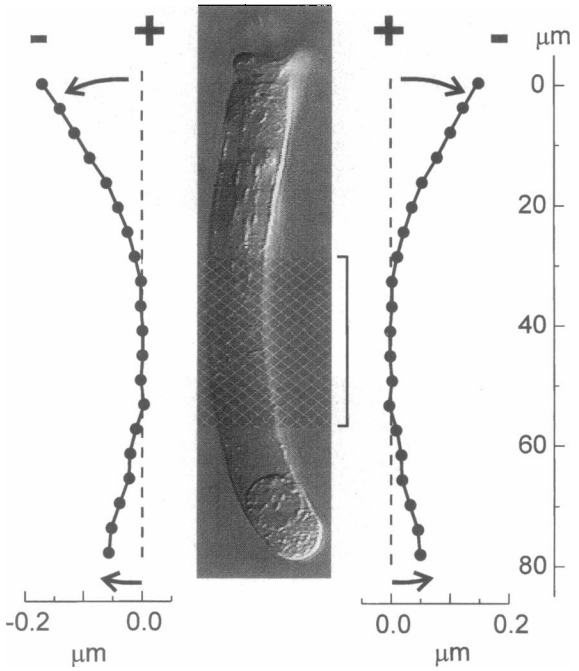

FIGURE 4 Displacements from the resting position of different points along the length of the OHC during electrically evoked bending motility. The dashed line represents the resting position. The plus and minus signs indicate the direction of the electric field. The bracketed area indicates the portion of the cell attached to the glass.

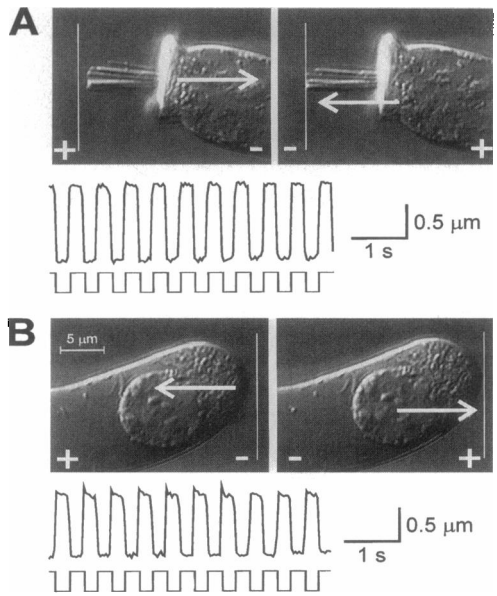

FIGURE 5 Electrically evoked longitudinal movements of apical (*A*) and basal (*B*) poles of the OHC. The images on the left of *A* and *B* were taken when current was passing from the left electrode to the right one (the electric field direction is marked by *plus and minus signs*). The images on the right side of *A* and *B* were taken when the electric field was passing from the right electrode to the left one. Arrows indicate the direction of movement relative to the vertical reference line. The measurement rectangle was aligned to quantify the movement along the *x* axis of the cuticular plate (*A*) and the synaptic pole (*B*). At the bottom of *A* and *B* we show the movements and the stimulating square pulses (2 Hz, 2 V, which produce potential gradients of ~1 mV/μm).

measured. The amplitude of the longitudinal movements was similar (±20%) to the amplitude of bending for 11 of the 27 cells, was lower for nine cells, and was greater for seven cells. In all cases where longitudinal motility was measured, OHCs contracted when the electric field was directed from cuticular plate to the basal region.

An accurate comparison of the movement amplitudes of the same cell at different orientations in the electric field was difficult, because the amplitude of the movements depended on how the cell was attached to the surface of the microscope slide. This attachment could be changed by electrical stimulation and disturbances during rotation of the microscope stage. Instead, we compared the linearity of OHC movement in the perpendicular and longitudinal electric fields. Fig. 6 shows the motile responses of an OHC attached to the glass surface by its middle portion. Motility was evoked by one sinusoidal cycle burst stimulation when the electric field was perpendicular to the cell's lateral wall and after 90° rotations of the microscope stage. The OHC bending response was typically symmetrical in relation to the resting position (Fig. 6) and was always more linear than the longitudinal movement (Fig. 6). In the longitudinal movement the displacement during the elongation phase was always larger than the displacement during contraction (Fig. 6).

Figs. 3, 4, and 6 illustrate the bending of cells that were attached to glass by their middle region or one of their ends. In Fig. 7 we show a cell that was tethered to the substrate in a way that most of the cell body was free to move. In this case, when the electric field was perpendicular to the cell body, the cell exhibited the bending motion, with the apical and basal ends moving in one direction and the middle of the cell moving in the other direction—in antiphase (Fig. 7, *A* and *B*, *middle panels*). When the electric field was made parallel to the cell body, the cell showed the characteristic contraction and elongation (Fig. 7 *C*).

To test whether electrically evoked OHC bending is a result of active force generation by the OHC, we recorded OHC motility before and after application of pCMPS or pHMPS. These reagents are known to block OHC electromotility (Kalinec and Kachar, 1993). The application of 1 mM pCMPS completely blocked electrically evoked bending and longitudinal motility (Fig. 7, *bottom*), as tested in 11 cells. pCMPS blocked both types of electrically evoked OHC motility within 5–10 min. Bending and longitudinal movements were also completely blocked by 1 mM pHMPS. Without sulfhydryl reagents, OHC electromotility persisted for more than 30 min of continuous electric stimulation.

DISCUSSION

We report here that in addition to the well-characterized elongation and contraction, OHC electromotility can generate forces that produce bending of the cell body. Bending

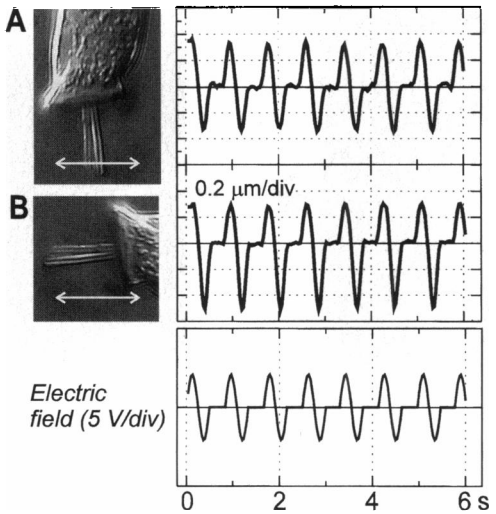

FIGURE 6 Nonlinearity of OHC motile response. (*A*) Bending motion of the apical part of the OHC in a perpendicular electric field. (*B*) Longitudinal movement after rotating the same cell 90°. Orientation of the electric field is indicated by the arrows. The stimuli consisted of sinusoidal pulses of 0.5 s duration, with a repetition rate of 1.2 Hz. The bottom trace shows the stimulating sinusoidal pulses of 2 Hz, 2 V, which produce maximum potential gradients of ~1 mV/μm.

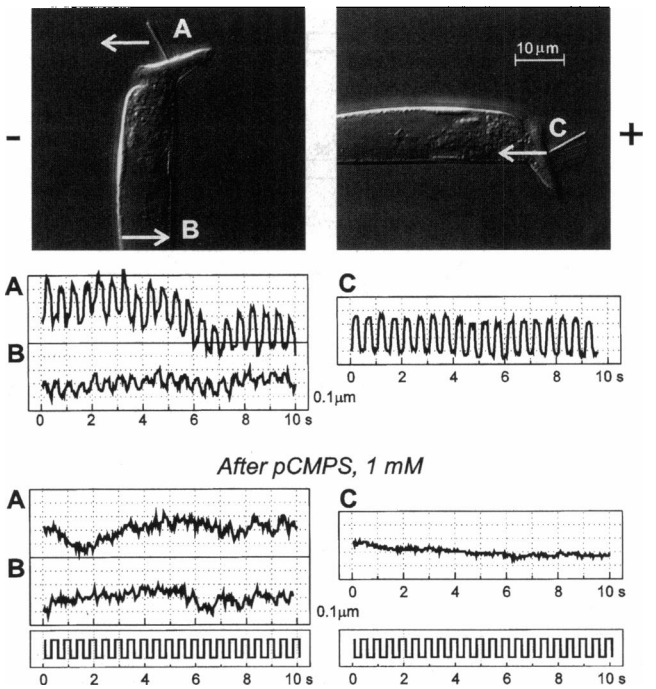

FIGURE 7 Electrically evoked movement in a floating OHC. Upper images show this cell in the perpendicular (*left*) and longitudinal (*right*) electric fields. Arrows indicate directions of motion of stereocilia (*A*) and lateral wall (*B*) in the perpendicular field, as well as cuticular plate motion (*C*) in the longitudinal field. Plus and minus signs indicate the direction of the electric field. Traces represent the *x* components of the movements. The records at the bottom show the movements of the same portions of the cell 14 min after application of 1 mM pCMPS. Changes in baselines are due to the slow rotation movements of the floating cell. The bottom traces are the stimulating square pulses of 2 Hz, 2 V, which produce potential gradients of ~1 mV/μm.

movements are produced when an isolated OHC is exposed to transcellular electric fields oriented perpendicular to its axis.

Because ionic currents in an electrolyte may entrain relatively large uncharged particles (Jerry et al., 1995), one could argue that the bending of an OHC attached to the glass substrate, as described here, could be a passive elastic flexion evoked by this electroosmotic flow. However, several factors rule out this possibility. We have always used currents well below the threshold for causing any visible electrophoretic flow of even the smallest debris floating in the fluid nearby the cells. Distinct bending motions could be observed in floating OHCs (Fig. 6) without visible lateral translation of the cell as a whole. And finally, the bending motion is suppressed by sulfhydryl reagents. In fact, the inhibitory action of sulfhydryl reagents on longitudinal and bending OHC motility suggests that the same mechanisms are responsible for both types of OHC motility.

Longitudinal OHC motility has been shown to be driven by changes in membrane potential (Santos-Sacchi and Dilger, 1988; Iwasa and Kachar, 1989; Dallos et al., 1991). The motor elements for this electromotility are built in as integral components of the lateral plasma membrane (Kalinec et al., 1992). Under patch-clamp conditions, when the whole cell membrane potential is driven by an external voltage, the cell responds with axial movements. The cylindrical cell body elongates when the cell hyperpolarizes and shortens when the cell depolarizes (Ashmore, 1987).

By analyzing the electromotility phenomenon in isolated membrane patches of the OHC lateral plasma membrane, it has been shown that hyperpolarization produces an increase in membrane area, and depolarization results in a decrease in membrane area (Kalinec et al., 1992). We have now observed that when the stimulating electric field has a component perpendicular to the cell axis, the cell responds with a bending motion. This bending motion may result from asymmetrical changes in the lateral plasma membrane potential and, consequently, asymmetrical membrane area changes. Any electrically conductive liquid compartment enclosed by a membrane with relatively high resistance undergoes charge separation in an electric field (Fig. 8). Such charge separation in an OHC could produce depolarization on one side of the cell with contraction of the plasma membrane, and hyperpolarization on the opposite side with elongation of the plasma membrane. The result would be a bending of the OHC toward the negative electrode (Fig. 8), as was observed in all OHCs in this study. This would occur without net changes in the intracellular potential if we accept that the two sides of the cell have equal conductances (Fig. 8). We cannot make the same assumption for the case of longitudinal motility, because the membranes that are facing the electric field are the apical and basal surfaces, which have different conductances (Kros, 1996), and therefore the intracellular potential is likely to change.

The proposed separation of charges may produce significant transmembrane potential changes. For example, the

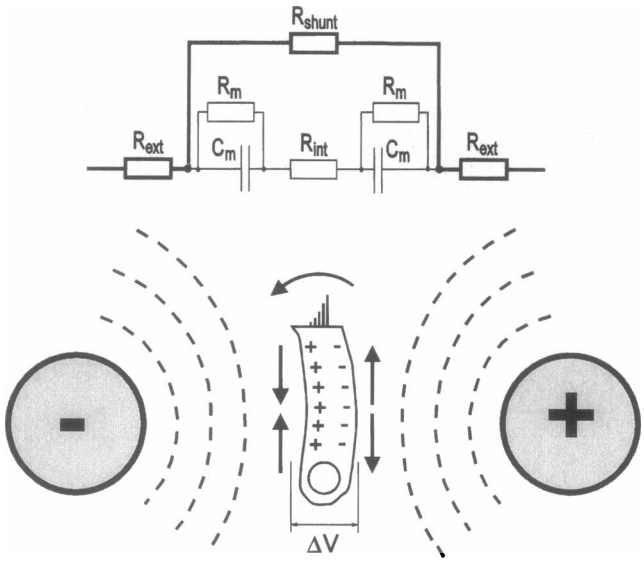

FIGURE 8 Mechanism of electrically evoked OHC bending (see text for explanation). Equivalent circuit elements: R_m, Resistance of lateral plasma membrane; C_m, capacitance of lateral plasma membrane; R_{int}, resistance of intracellular compartment; R_{ext}, resistance of extracellular pathway; R_{shunt}, shunting resistance of the pathways around OHC. Because $R_m \gg R_{shunt}$, the current passes mainly around the cell. Therefore the voltage drop across the cell diameter is not significantly influenced by the presence of the cell.

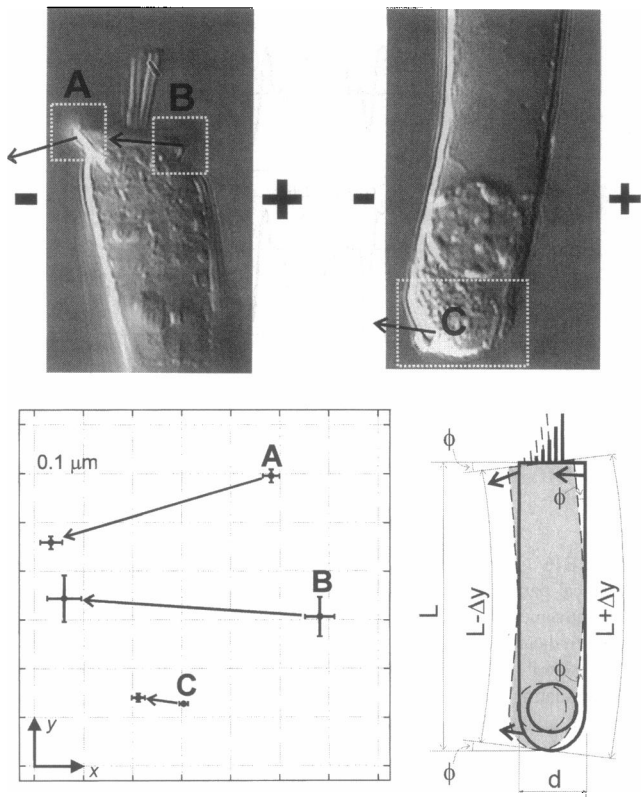

FIGURE 9 Correspondence of OHC bending motion displacement vectors to the model prediction. The video frames show images of OHC with displacement vectors for arbitrary tracking points on both sides of the cuticular plate (*A* and *B*) and on the nuclear pole (*C*) when a perpendicular electric field is applied from the right to the left of the cell body. The bottom panel shows in an expanded scale the averaged displacement (*arrows*) for 10 cycles. The positions of points *A* and *B* were determined by a 4-μm box of pixels centered at these arbitrary points. For point *C* we used a 4 μm × 10 μm rectangle. The schematic drawing in the bottom right panel represents the predicted displacement vectors. The opposite sides of the lateral wall of a bent OHC were drawn as circle segments of different lengths. The apical and basal poles of the cell bend synchronously by a small angle ϕ around a point in the middle of the OHC.

bending of the OHC illustrated in Fig. 3 was driven by a voltage gradient of ~1 mV/μm. Taking into account the cell diameter (10 μm), this corresponds to a voltage difference across the diameter of the cell (ΔV) of ~10 mV (Fig. 8). Because the resistance of an intracellular compartment (R_{int}) is some orders of magnitude lower than the plasma membrane resistance (R_m), and the resistances of the left and right lateral membranes are about equal, the voltage difference across the cell is about equally divided between two sides. Thus, according to these conditions, the applied electric field evoked a 5-mV depolarization step on one side of the cell and a 5-mV hyperpolarization on the other side. Assuming the typical mechanical response of long OHCs to be ~20 nm/mV of transmembrane potential (Ashmore, 1987), a long OHC would show a 0.1-μm contraction on one side and a 0.1-μm elongation on the other side. The total length difference between the lateral walls introduced by the electric field would be 0.2 μm. The voltage values used are not corrected for disturbance of the electric field by the OHC, which could increase our estimations by a factor of up to 2 (Jerry et al., 1996). On the other hand, we did not account for the curvature of the cylindrical cell wall, which would also decrease the estimations by a factor of ~2. In the ideal case of a straight cylindrical cell body and uniform distribution of motor elements along the cell's lateral wall, the OHC would bend around a point in the middle (Fig. 9, *right bottom panel*), and a difference in lateral wall length (Δy, Fig. 9) would be divided equally between the apical and basal parts of the OHC. This would produce bending of the apical and basal parts of the OHC through a small angle $2\phi = 2\,\Delta y/d = 2 \times 0.1/10 = 0.02$ radians total (Fig. 9). Our experimental results illustrated in Fig. 4 are in agreement with these calculations.

The voltage-driven length changes at the opposite sides of the OHC lateral wall can be measured directly. Fig. 9 shows the same cell as Fig. 3, where displacement measurements were made at two opposite regions (*A*, to the left, and *B*, to the right) of the cuticular plate. Displacement vectors were obtained for these two regions (Fig. 9), which agree with what would be expected during bending of the apical part of the cell through a small angle. Because the angle of bending is small, the difference in the lateral wall lengths induced by the electric field can be taken as the difference of the *y* components of the displacements of *A* and *B* (Fig. 9). The value that we obtained for the cell shown in Fig. 8 was 0.18 μm, which corresponds to excursions of 0.09 μm from the resting position. This value is consistent with the 0.2 μm value estimated above. Because the image of the

nuclear pole of the OHC does not have sharp edges like the image of the apical pole, the measurements of the displacement vectors for this region were more difficult to determine. Nevertheless, the direction of the nuclear pole displacement vector was consistent with predictions (Fig. 9).

Nonlinearity of OHC motility in an external electric field

Isolated OHCs show clear asymmetries in voltage-dependent length changes. Thus, under whole-cell patch-clamp conditions with a holding potential of around −70 mV, the elongation response to hyperpolarizing potential steps is close to saturation, whereas the contraction response is linear over a broad range of depolarizing voltage steps (Santos-Sacchi, 1989). We observed the opposite relationship for longitudinal OHC motility in an external electric field (Fig. 5). This is not surprising, because there is strong evidence that isolated OHCs in culture medium are depolarized as compared to in vivo conditions (Ashmore, 1987; Santos-Sacchi and Dilger, 1988). Indeed, the motile response of an OHC with an intracellular potential of −40 mV, which is quite common for isolated cells (Santos-Sacchi and Dilger, 1988), is more saturated in the depolarizing direction than in the hyperpolarizing direction (Ashmore, 1987).

Our model suggests that a perpendicular electric field evokes equal depolarization and hyperpolarization voltage changes on the opposite sides of a cell. These changes could produce nonequal contraction and elongation between the left and right sides of the OHC lateral wall. The resulting bending would be proportional to the sum of these contraction and elongation displacements of each side of the lateral wall. An opposite electric field would cause bending of the same amplitude, but in the opposite direction. In accordance with this consideration, electrically evoked bending was more linear than longitudinal OHC motility (Fig. 5).

OHC bending as a way to study fast OHC motility

All of our evidence suggests that OHC bending evoked by a perpendicular electric field is a manifestation of voltage-dependent OHC motility. This form of evoking OHC electromotility has some advantages as an experimental model, especially for pharmacological studies in which a large number of cells must be tested. First, an external electric field is the easiest way to evoke fast OHC motility. Second, OHC bending is more predictable than OHC motility in a longitudinal electric field. However, bending displacements are smaller than longitudinal displacements under patch-clamp conditions, and driving potential changes are easier to control in patch-clamp or microchamber conditions.

The physiological significance of OHC bending

Does the external electric field modify OHC motility in vivo? At low frequencies, sound-induced potential changes in the extracellular space at points close to the OHC basolateral wall are about one order of magnitude less than potential changes inside the OHC (Kossl and Russell, 1992). Thus, at low frequencies, the effect of an external electric field could be insignificant. However, at high frequencies, the intracellular sound-induced voltage response is severely attenuated because of resistance-capacitance filtering of the cell membrane (Santos-Sacchi, 1992), and extracellular sound-induced responses could become comparable to or even bigger than intracellular ones (Dallos and Evans, 1995). It is known that extracellular potential changes can effectively drive the motility of isolated OHCs at high frequencies up to 22 kHz (Dallos and Evans, 1995).

An external electric field can also produce prominent radial movement of OHC cuticular plates in the whole organ of Corti preparation, even at high frequencies (Reuter et al., 1992). Part of this radial motion may be related to active OHC bending, because the placement of electrodes in these studies cannot exclude the presence of an extracellular electric field component perpendicular to the OHCs.

It is not known whether a radial component that could drive OHC bending exists in vivo in sound-induced extracellular electric fields. A 200-Hz acoustic stimulation can produce a radial voltage gradient of ~6 mV/mm in scala tympani, far below the organ of Corti (Zidanic and Brownell, 1990). The length constant of exponential decay of the microphonic potential in the scala media is ~1 mm (Johnstone et al., 1966). However, nothing is known about the local extracellular electric fields inside the organ of Corti, below the reticular lamina. For example, the endocochlear potential must produce paracellular leakage currents across the reticular lamina, through the tight junctions, and around the hair cells and supporting cells. We do not know how these currents are distributed in relation to the cylindrical cell bodies of the OHCs, which are positioned at an angle in relation to the reticular lamina. Therefore, OHCs could indeed be exposed to transverse electric fields and generate active radial forces in the organ of Corti. These forces may be weak in comparison with the longitudinal forces and contribute little to the distortion of the organ of Corti. However, they can be effective in disturbing the mechanosensitive lateral wall of the OHC (Iwasa et al., 1991; Ding et al., 1991) and stereocilia bundle as well as other internal cytoplasmic structures. On the other hand, persistent or repeated electrically induced bending could also produce long-term plastic changes in the OHC. It is interesting to note that OHCs quite often show a slightly bent cell body.

We thank Drs. Don Coling, Jorgen Fex, and Richard Chadwick for critically reading the manuscript.

REFERENCES

Ashmore, J. F. 1987. A fast motile response in guinea-pig outer hair cells: the cellular basis of the cochlear amplifier. *J. Physiol. (Lond.).* 388: 323–347.

Brownell, W. E., C. R. Bader, D. Bertrand, and Y. Ribaupierre. 1985. Evoked mechanical responses of isolated cochlear outer hair cells. *Science.* 227:194–196.

Brownell, W. E., and B. Kachar. 1985. Outer hair cell motility: a possible elctrokinetic mechanism. *In* Auditory Biomechanics. J. B. Allen et al., editors. Springer Verlag, New York. 369–376.

Dallos, P., and M. A. Cheatham. 1992. Cochlear hair cell function reflected in intracellular recordings in vivo. *Soc. Gen. Physiol. Ser.* 47:371–393.

Dallos, P., and B. N. Evans. 1995. High-frequency motility of outer hair cells and the cochlear amplifier. *Science.* 267:2006–2009.

Dallos, P., B. N. Evans, and R. Hallworth. 1991. Nature of the motor element in electrokinetic shape changes of cochlear outer hair cells. *Nature.* 350:1–3.

Ding, J. P., R. J. Salvi, and F. Sachs. 1991. Stretch-activated ion channels in guinea pig outer hair cells. *Hear. Res.* 56:19–28.

Evans, B. N., and P. Dallos. 1993. Stereocilia displacement induced somatic motility of cochlear outer hair cells. *Proc. Natl. Acad. Sci. USA.* 90:8347–8351.

Evans, B. N., R. Hallworth, and P. Dallos. 1991. Outer hair cell electromotility: the sensitivity and vulnerability of the DC component. *Hear. Res.* 52:288–304.

Hallworth, R., B. N. Evans, and P. Dallos. 1993. The location and mechanism of electromotility in guinea pig outer hair cells. *J. Neurophysiol.* 70:549–558.

Iwasa, K. H., and B. Kachar. 1989. Fast in vitro movement of outer hair cells in an external electric field: effect of digitonin, a membrane permeabilizing agent. *Hear. Res.* 40:247–254.

Iwasa, K. H., M. Li, M. Jia, and B. Kachar. 1991. Stretch sensitivity of the lateral wall of the auditory outer hair cell. *Neurosci. Lett.* 133:171–174.

Jerry, R. A., A. S. Popel, and W. E. Brownell. 1995. Outer hair cell length changes in an external electric field. I. The role of intracellular electro-osmotically generated pressure gradients. *J. Acoust. Soc. Am.* 98: 2000–2010.

Jerry, R. A., A. S. Popel, and W. E. Brownell. 1996. Potential distribution for a spheroidal cell having a conductive membrane in an electric field. *IEEE Trans. Biomed. Eng.* 43:970–972.

Johnstone, B. M., J. R. Johnstone, and I. D. Pugsley. 1966. Membrane resistance in endolymphatic walls of the first turn of the guinea pig cochlea. *J. Acoust. Soc. Am.* 40:1398–1404.

Kachar, B., P. C. Bridgman, and T. S. Reese. 1987. Dynamic shape changes of cytoplasmic organelles translocating along microtubules. *J. Cell Biol.* 105:1267–1271.

Kachar, B., W. E. Brownell, R. Altschuler, and J. Fex. 1986. Electrokinetic shape changes of cochlear outer hair cells. *Nature.* 322:365–367.

Kalinec, F., M. C. Holley, K. H. Iwasa, D. J. Lim, and B. Kachar. 1992. A membrane-based force generation mechanism in auditory sensory cells. *Proc. Natl. Acad. Sci. USA.* 89:8671–8675.

Kalinec, F., and B. Kachar. 1993. Inhibition of outer hair cell electromotility by sulfhydryl specific reagents. *Neurosci. Lett.* 157:231–234.

Kolston, P. J. 1995. A faster transduction mechanism for the cochlear amplifier? *Trends Neurosci.* 18:427–429.

Korn, G. A., and T. M. Korn. 1968. Mathematical Textbook for Scientists and Engineers. McGraw-Hill, New York.

Kossl, M., and I. J. Russell. 1992. The phase and magnitude of hair cell receptor potentials and frequency tuning in the guinea pig cochlea. *J. Neurosci.* 12:1575–1586.

Kros, C. J. 1996. Physiology of mammalian cochlear hair cells. *In* The Cochlea. P. Dallos, A. N. Popper, and R. R. Fay, editors. Springer Verlag, New York. 318–385.

Patuzzi, R., and D. Robertson. 1988. Tuning in the mammalian cochlea. *Physiol. Rev.* 68:1009–1082.

Reuter, G., A. H. Gitter, U. Thurm, and H. P. Zenner. 1992. High frequency radial movements of the reticular lamina induced by outer hair cell motility. *Hear. Res.* 60:236–246.

Santos-Sacchi, J. 1989. Asymmetry in voltage-dependent movements of isolated outer hair cells from the organ of Corti. *J. Neurosci.* 9:2954–2962.

Santos-Sacchi, J. 1992. On the frequency limit and phase of outer hair cell motility: effects of the membrane filter. *J. Neurosci.* 12:1906–1916.

Santos-Sacchi, J., and J. P. Dilger. 1988. Whole cell currents and mechanical responses of isolated outer hair cells. *Hear. Res.* 35:143–150.

Spoendlin, H. 1970. Structural basis of peripheral frequency analysis. *In* Frequency Analysis and Periodicity Detection in Hearing. R. Plomp and G. F. Smoorenburg, editors. Sijthoff, Leiden. 2–40.

von Békésy, G. 1960. Experiments in Hearing. McGraw-Hill, New York.

Zenner, H. P., U. Zimmermann, and U. Schmitt. 1985. Reversible contraction of isolated mammalian cochlear hair cells. *Hear. Res.* 18:127–133.

Zidanic, M., and W. E. Brownell. 1990. Fine structure of the intracochlear potential field. I. The silent current. *Biophys. J.* 57:1253–1268.